ADVANCED MATERIALS
www.advmat.de

# Programmable Robotic Shape Shifting and Color Morphing Dynamics Through Magneto-Mechano-Chromic Coupling

*Xueling Li, Yin Cheng,* Yi Zhou, Liangjing Shi, Jing Sun, Ghim Wei Ho,* and Ranran Wang**

**Recreating natural organisms' dynamic shape-morphing and adaptive color-changing capabilities in a compact structure poses significant challenges but unlocks unprecedented hybridized robotic-visual applications. Overcoming programmability and predictability obstacles is key to achieving real-time, responsive changes in appearance and functionality, enhancing robot-environment-user interactions in ways previously unattainable. Herein, a Soft Magneto-Mechano-Chromic (SoMMeC) structure comprising a magnetic actuating and a synthetic photonic film, mirroring the intricate color-tuning mechanism of chameleons is devised. A model combining numerical simulation and a strain-dependent color evolution map enables precise predictions and controllable shape-color alterations across various geometrical and magnetization profiles. The SoMMeC exhibits rapid (0.1s), broad (full-visible spectrum), tether-free (remote magnetic manipulation), and programmable (model-guided control) color transformations, surpassing traditional limitations with its real-time response, broad and omnidirectional coloration for enhanced visibility, and robustness against external disturbances. The SoMMeC translates into dynamic advertising iridescence, adaptive camouflage, self-sensing, and multi-level encryption, and transcends traditional robotics by seamlessly blending dynamic movement with nuanced visual changes. It opens up a spectrum of applications that redefine robotic functionality through dynamic appearance modulation, making robotic systems more versatile, adaptive, and suitable for unexplored integrative functions.**

## 1. Introduction

Many biological organisms have evolved two critical traits of shape-morphing and color-changing to gain survival advantages: The Venus flytrap is capable of rapidly closing up the leaves to prey insects;[1] The stick insect changes body color to disguise itself from predators.[2] Scientists and engineers have long strived to imitate the two biological merits to develop functional materials. Soft robots have borrowed the idea of compliant shape-morphing for adaptive manipulation or locomotion,[3–7] and proved effective in broad applications of grippers,[8–10] human-machine interactive platform,[11,12] and biomedical mini-robots.[13,14] Besides, different color-changing strategies have been employed in applications of smart display,[15,16] visualized sensing,[17,18] anti-counterfeiting and encryption.[19,20]

However, such singular shape- or color-transformation failed to achieve simultaneous modulation in appearance and functionality. In order to enhance robot-environment and robot-user interactions for hybridized robotic-visual applications, there have been some attempts aimed at integrating shape-shifting and color-morphing. In a pioneering work, Morin et al., devised a pneumatic soft robot equipped with microfluidic dyed liquids to realize skin color changes.[21] However, pumping the liquid flow deterred fast color change and tether-free locomotion.[22] Fluorescent hydrogel actuators achieved various stimuli-triggered fluorescence, such as temperature,[23] metal ions,[24] and pH value.[25] Nevertheless, the underlying ion permeation or heat transfer in hydrogel matrix featured slow kinetics, causing a considerably extended color-response time of up to several minutes.

X. Li, Y. Cheng, L. Shi, J. Sun, R. Wang
The State Key Laboratory of High Performance Ceramics and Superfine Microstructure
Shanghai Institute of Ceramics
Chinese Academy of Science
Shanghai 200050, China
E-mail: chengyin@mail.sic.ac.cn; wangranran@mail.sic.ac.cn

The ORCID identification number(s) for the author(s) of this article can be found under https://doi.org/10.1002/adma.202406714

DOI: 10.1002/adma.202406714

X. Li
School of Microelectronics
Shanghai University
Shanghai 200444, China

Y. Zhou, G. W. Ho
Department of Electrical and Computer Engineering
National University of Singapore
4 Engineering Drive 3, Singapore 117583, Singapore
E-mail: elehgw@nus.edu.sg

R. Wang
School of Chemistry and Materials Science
Hangzhou Institute for Advanced Study
University of Chinese Academy of Sciences
1 Sub-lane Xiangshan, Hangzhou 310024, China

 

Electro- and mechano-luminescence could afford an almost instant color change. Larson et al., combined a pneumatic crawling robot with a multi-pixeled electroluminescent (EL) skin based on ZnS phosphor dielectric.[26] Unfortunately, the predetermined metal doping in phosphor resulted in hue-fixed coloration for each pixel, rather than a dynamic spatiotemporal tuning.[27,28] Thermotropic cholesteric liquid crystal elastomers possess the desirable heat-induced deformation and color change. Nonetheless, these liquid crystal robots required a prohibitively high temperature to trigger the shape-color change (typically above 80 °C),[29,30] and necessitated an extra complex temperature-control system to cope with the ambient temperature fluctuation.[31] Vapochromic actuators with inverse opal structures proved to be effective strategy to exhibit fast and dynamic color change,[32–35] yet they were incompetent to offer stably accessible hues and robust hue control during actuation, hindering the accurate shape-color programming. Currently, it remains a formidable challenge to develop a robotic structure with not only fast and broad hue changes, but also spatiotemporally dynamic and coupled tuning for real-time robot-environment and robot-user interactions, which promises more sophisticated robotic, sensing, and encryption applications. Magnetically triggered mechanical response is a promising avenue toward complex shape morphing and locomotion considering the fast, remote, and highly programmable actuating features. The magneto-mechano effect has been incorporated with triboelectric or electromagnetic effect to design flexible nanogenerator for biomechanical energy harvesting.[36–38] Besides, the luminescence effect could be driven by magneto-mechano imput to achieve real-time visualization and remote sensing.[39,40] Till now, magnetic control over shape-color tunability is still unexplored.

Herein, by mimicking the mechanism of chameleon's active skin coloration through lattice tuning of guanine nanocrystals in dermal iridophore, we devise an entirely soft magneto-mechano-chromic (SoMMeC) structure consisted of a photonic crystal (PC) film and a magnetic actuator. The SoMMeC robots offer a fast (≈0.1s), broad (full-visible-spectrum) and tether-free (remote magnetic control) shape-color change through a synergistic magneto-mechano-chromic (MMC) coupling mechanism. We developed a model combining numerical simulation and a strain-dependent color evolution map, to allow precise predictions and programmable shape-color alterations across various geometrical and magnetization profiles. To demonstrate the versatility of SoMMeC structures in robotic-visual applications, we showcased locomotive robots with dynamic advertising iridescence and adaptive self-camouflage, a soft gripper with visual-feedback, and a pixelated encoding disk with advanced encryption. The SoMMeC structure holds great potential in future self-camouflaged robots, self-feedback robotic sensing, and high-security visual cryptography.

## 2. Results

### 2.1. Design of SoMMeC Structure and Predictive Model of MMC Coupling

Conventional soft robots featured a singular stimulus-responsive structure, which provided a shape adjustment without appearance (surface color) modification (**Figure 1a**). Chameleons have the skill to rapidly change their body color (hue) during locomotion, owing to the active neuromuscular tuning of guanine nanocrystal spacing.[41] We devised a biomimetic SoMMeC structure composed of a synthetic PC layer (non-close-packed $SiO_2$ nanospheres in an acrylate matrix with a thickness of ≈50 µm) and a magnetic actuating layer (NdFeB microparticles in PDMS with a thickness of ≈1 mm) (Figure S1, Supporting Information). Upon magnetic stimulus, the SoMMeC structure went through a programmable shape-morphing due to the magnetic torque and/or magnetic force.[42,43] The shape-morphing leads to bending deformations accompanied by surface compressive or tensile lateral strain, resulting in an active tuning of the PC lattice spacing to realize the shifting of the photonic bandgap. This ingenious SoMMeC structure couples the localized surface strain to the dynamic shaping and coloration, distinct from conventional soft robots (Figure 1b).

We developed a predictive model to analyze the synergistic MMC coupling (Figure 1c; Note S1, Supporting Information). First, numerical simulation (finite element analysis, FEA) was implemented to obtain the shape change and surface strain mapping under the magnetic stimulus. Due to the huge rigidity discrepancies between the silica particle (Young's modulus of ≈70 GPa) and the acrylate matrix (Young's modulus of 0.175 MPa), the applied strain is almost completely transferred to the soft matrix, while the silica particles maintain the original dimensions (detailed experimental and simulation analysis in Figure S2, Supporting Information). Then, the strain-dependent color evolving map was established via physical derivation and confirmed by experiments (discussed later). Lastly, by combining the simulation results and the color-evolving map, the shape-color transformation could be predicted. This model is beneficial for the theoretical optimization of the design parameters of SoMMeC structures for different usages. For instance, the SoMMeC robot could generate stably accessible multi-hues during actuation: a disk-shaped SoMMeC structure with radial magnetization exhibits stable and controllable surface colors of up to seven distinct hues (Figure 1d; Figure S3, Supporting Information). Besides, the highly elastic actuating layer dominated the magnetic deformation to deliver an ultrafast (less than 0.1s response time) and synchronized chape-color alteration, exemplified by a SoMMeC-based flower blooming (Movie S1, Supporting Information). Compared with the state-of-the-art color-changeable robots, our SoMMeC robot ranks at the highest level in terms of the response time of hue change and stably accessible hues (Figure 1e). More importantly, the MMC coupling mechanism enables a spatiotemporally dynamic hue tuning and coupled morphing-coloration behavior through a single magnetic control (Figure 1f and detailed information in Table S1, Supporting Information).

### 2.2. The photonic Crystal Films

A PC film composed of silica particle colloids was fabricated as the color-changing element. It offers several advantages over dyed or pigmentary colors, including long-term stability, environmental friendliness, and most importantly, dynamic spatiotemporal tunability.[44–46] Monodisperse silica particles self-assembled into a non-close-packed face-centered-cubic (fcc)

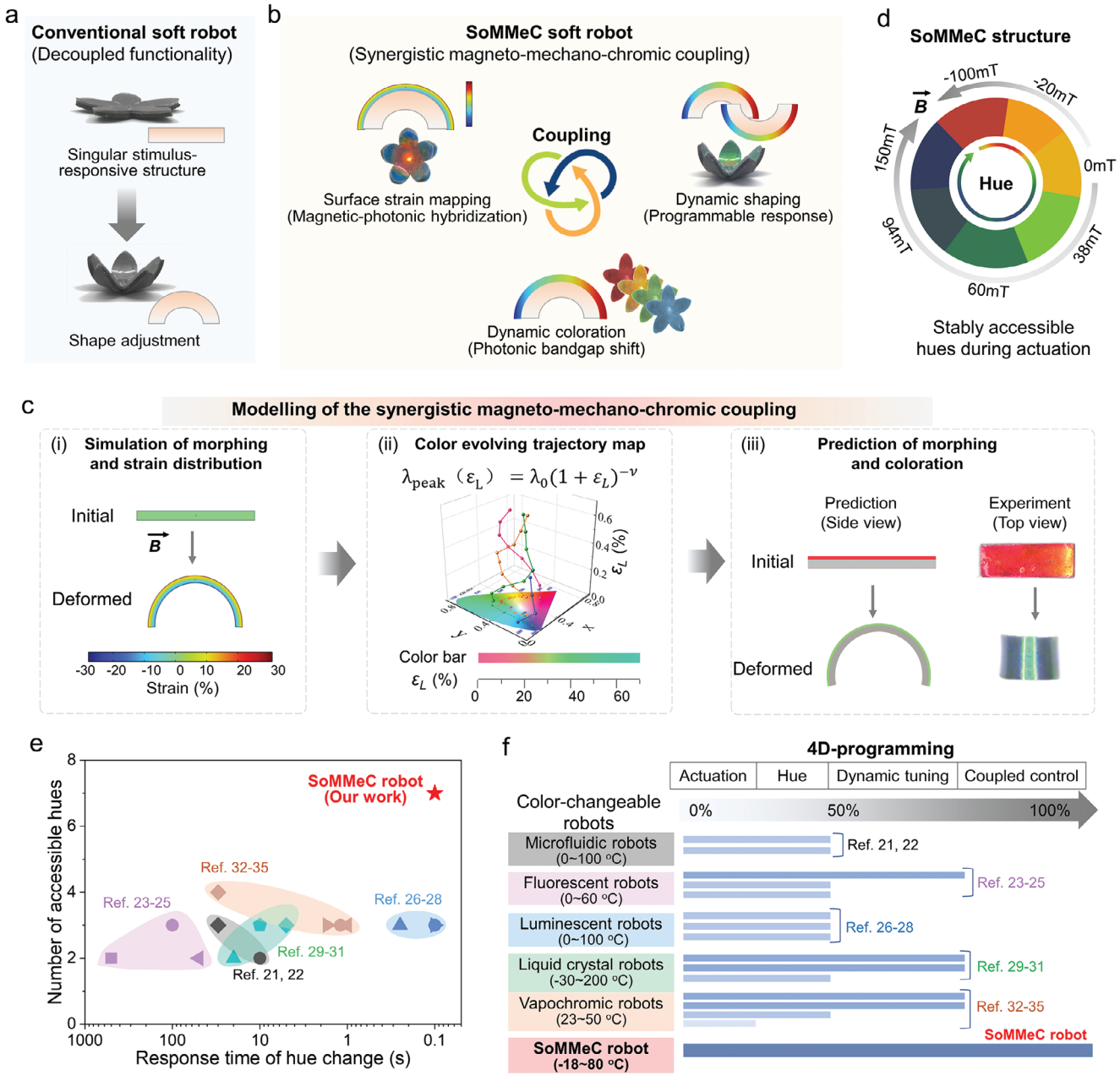


**Figure 1.** The design of SoMMeC structure with MMC coupling. a) Conventional soft robot with singular stimulus-responsive structure. b) The synergistic MMC coupling of SoMMeC robot, including magnetic shaping, shaping-induced surface strain mapping, and dynamic coloration induced by photonic bandgap shifting. c) The modeling of the synergistic SoMMeC coupling. Including the simulation of morphing and strain distribution i), the color-evolving trajectory map establishment ii), and the prediction of the shape-morphing and color-changing iii). d) Stably accessible hues of a SoMMeC rolling robot during magnetic actuation. e) Comparison with the state-of-the-art color-changeable robots in terms of the response time of hue change and stably accessible hues during actuation. f) 4D programming (actuation, hue, spatiotemporally dynamic tuning, and coupled control) evaluation of reported color-changeable robots and our SoMMeC robot. The widest possible operation temperature ranges for the different types were summazied for performance comparison, which were extracted from testing conditions or infered from compositional materials of these color-changable robots.

lattice in a rubber precursor of polyethylene glycol phenyl ether acrylate (PEGPEA) and di(ethylene glycol) ethyl ether acrylate (DEGEEA), and were immobilized within the elastomeric matrix via rapid photocuring (Figure S4, Supporting Information). The non-close-packing stemmed from the interparticle repulsion due to the hydrogen bonding between the silanol groups and the acrylate groups, as affirmed by Fourier transform infrared spectroscopy (FTIR) and variable-temperature FTIR (25-85 °C) results (Figure S5, Supporting Information). The non-close-packed arrangement afforded sufficient lattice tuning space for wide-range color change under tensile or compressive lateral strains.

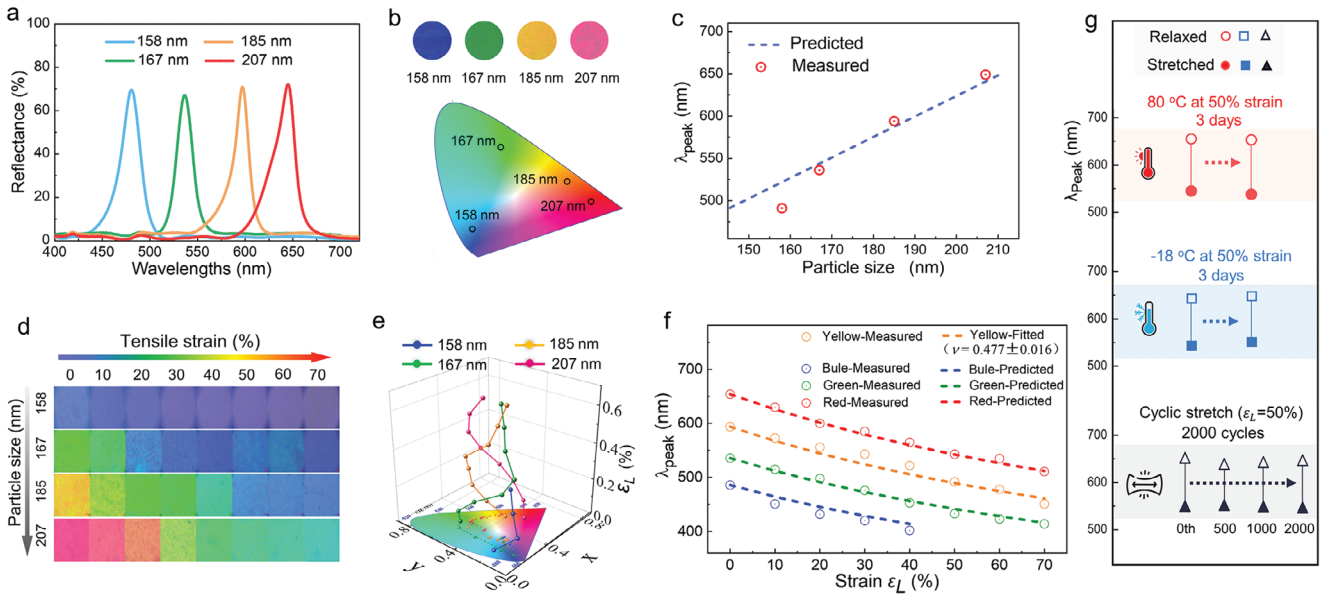


**Figure 2.** Properties of the PC film and the strain-dependent color evolving map. a) Reflection spectra of PC films with varied particle sizes (158, 167, 185, and 207 nm). b) Digital photographs of the PC films with different particle sizes (top) and the corresponding coordinates in the CIE chromaticity diagram (bottom). c) The measured (hollow circles) and predicted (dotted line) reflectance peaks of PC films with varied particle sizes. d) Photographs of PC films with varied particle sizes under a tensile strain of up to 70%. e) The strain-dependent color evolving trajectory map of PC films with different initial hues. f) The measured (hollow circles) and predicted (dotted lines) reflectance peak shifting under an increasing lateral strain. g) The reflectance peaks of PC films at initial and strained states through extreme temperature and cyclic stretch tests.

$SiO_2$ nanospheres with different sizes were prepared by a modified Stöber method (Figure S6, Supporting Information). At a constant silica volume fraction of 25%, the resultant PC films exhibited tailorable reflection peaks of 486 nm (blue hue), 536 nm (green), 594 nm (yellow), and 654 nm (red) at normal reflection with particle sizes of 158, 167, 185, and 207 nm, respectively (**Figure 2a**). The photonic films showed bright colors owing to the high reflectance of 70%, validated by the border-approaching positions of the mapped color points in a CIE (International Commission on Illumination) chromaticity diagram (Figure 2b). The bandgap position $\lambda_{peak}$ can be calculated using Bragg's equation for a normal-incident light on the close-packed plane of an fcc structure:[47]

$$\lambda_{peak} = 2d\, n_{eff} = \sqrt{\frac{8}{3}}\, Dn_{eff} \quad (1)$$

$$n_{eff}^2 = \Sigma n_i^2 V_i \quad (2)$$

Here, $\lambda_{peak}$ is the wavelength of the reflectance peak, $d$ the spacing between the close-packed planes, $n_{eff}$ the effective refractive index, $D$ the interparticle distance, and $n_i$and $V_i$ represent the refractive index and volume fraction of the components in the PC film respectively. Based on this model, Figure 2c displays the measured silica particle size dependence of the reflectance peak, which agrees well with the model-based calculation, proving the non-close-packed ordered fcc structure. The adoption of homogenous silica particles with other varying size could expand the color palette of the PC films, and the particle volume ratio in the matrix is another effective factor to regulate the initial hues (particle size of 200 nm as an example in Figure S7, Supporting Information). To favor a decent range of lattice spacing variation for wide color-tuning, we here selected a constant silica volume fraction of 25%. The PC films of varying initial hues were subjected to gradually increased tensile strain up to 70% (Figure 2d). The color all experienced a blueshift in spectral reflectance (Figure S8, Supporting Information), due to the vertical shrinking of lattice spacing caused by the lateral elongation. The color trajectories were visualized by mapping each measured reflectance spectrum to a point in the CIE color space, thus establishing a strain-dependent color-evolving trajectory map (Figure 2e). To achieve a generalized relationship between the color and applied strain, we adopted a linear-elastic mechanical model based on approximate Poisson's ratio $\nu$ of the material as seen in Equation (3)[17]

$$\lambda_{peak}\left(\varepsilon_L\right) = \lambda_0\left(1+\varepsilon_L\right)^{-\nu} \quad (3)$$

Here, $\lambda_0$ and $\lambda_{peak}(\varepsilon_L)$ are the peak reflection wavelengths at initial and strained (applied lateral strain $\varepsilon_L$) states, respectively. In Figure 2f, a PC film with a yellow hue was used for model evaluation, and a well-matched fitting between the measured strain-dependent peak wavelengths and the fitted power law relation was observed, giving an estimated Poisson's ratio value of 0.477±0.016. Further comparison between the predicted curves (dotted lines) and the measured data (hollow circles) from other hues showed a close match, corroborating the quantitative prediction of the photonic bandgap shifts upon applied strains. As the bending-induced actuation strain of the SoMMeC structure directly determines the hue response of the PC film, the bending curvature and the thickness collectively influence the color-tuning performance. Based on the Euler–Bernoulli theory as an approximate analysis, larger curvature and thickness

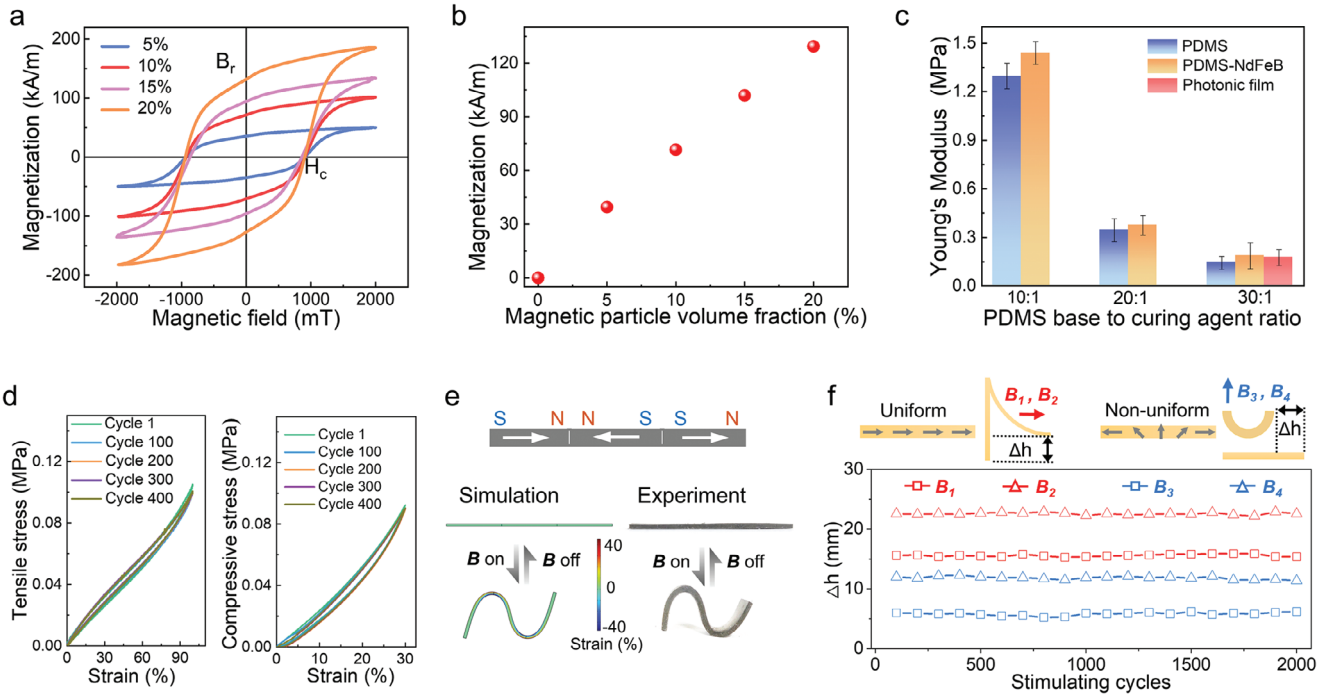


**Figure 3.** The magnetic and mechanical properties of the magnetic actuating layer. a) Magnetic hysteresis loops of PDMS-NdFeB composites with varying NdFeB volume fractions. *Hc* and *Br* indicate the coercive force and remnant magnetization. b) The magnetization magnitude of PDMS-NdFeB composites with varying NdFeB volume fractions. c) The Young's modulus of PDMS, PDMS-NdFeB composites, and the PC film. d) The cyclic tensile and compressive stress–strain curves of the PDMS-NdFeB composite. e) Simulation and experiment results of a sheet sample under a magnetic field of 100 mT. Sample size of 25 mm × 5 mm × 1 mm. f) The actuation stability of a PDMS-NdFeB sheet with uniform (35 mm × 5 mm × 1 mm) and nonuniform (18 mm × 5 mm × 1 mm) magnetizations.

of the SoMMeC structure contribute to increased tensile strain on the upper surface, leading to the blueshift of the photonic bandgap for the PC film (detailed discussion in Note S2, Supporting Information). The thermal and mechanical robustness of the color tunability was assessed under harsh testing conditions. We measured the reflective peak wavelengths of PC film samples at relaxed and stretched ($\varepsilon_L$ of 50%) states after storage under 80 °C/−18 °C for 3 days at a stretched state (50%), and 2000 stretching cycles (50%). Figure 2g summarizes the $\lambda_{peak}$ at relaxed and stretched states before and after each test (Figure S9, Supporting Information), suggesting remarkable mechano-photonic robustness under thermal and mechanical impacts. The reflection spectra of the PC film at relaxed and stretched (50%) states were shown in Figure S10 (Supporting Information), with the color variation mapped in the CIE chromaticity diagram during 2000 stretching cycles. The two clusters of color points verified a high color-tuning stability. Besides, the PC films of different hues exhibited vivid and almost consistent colors after one year of storage in the ambient environment (Figure S11, Supporting Information).

### 2.3. The Magnetic Actuating Layer

A soft composite of hard-magnetic neodymium iron boron (NdFeB) particles and polydimethylsiloxane (PDMS) matrix was employed to serve as the actuating element considering its fast response, untethered control, and magnetization programmability.[48,49] **Figure 3a** shows the magnetization hysteresis curves of the composites containing different volume fractions of NdFeB particles, revealing high remnant magnetization and coercive force as desired. The extracted magnetic moment density in Figure 3b depicts a linear dependence on the volume fraction, varying from 39.5 to 129.3 kA $m^{-1}$. A 15% vol% was adopted for the magnetic actuating layer as it accommodated both a relatively high magnetization value (101.9 kA $m^{-1}$) and a favorable rheological behavior for easy NdFeB particle dispersion (the cross-sectional SEM image in Figure S12, Supporting Information). We conducted tensile stretch tests to PDMS with varying weight ratios of PDMS base to curing agent (10:1, 20:1, and 30:1), the magnetic counterparts (PDMS-NdFeB), and the PC film (Figure S13, Supporting Information). The 30:1 ratio was used for the fabrication of the magnetic actuating layer, as it possessed a similar Young's modulus and rupture strain to the PC film (Figure 3c), which favored the mitigation of the interfacial mechanical mismatch and shear stress concentration. Besides, its relatively low flexural rigidity contributed to a less demanding magnetic field strength to drive shape transformations. As shown in Figure 3d, the PDMS-NdFeB exhibited minimal residual strains and almost overlapped stress-strain curves during 400 cycles of tensile and compressive loading-unloading tests.

As an illustrative example to demonstrate the magnetically controlled shape-morphing, a PDMS-NdFeB sheet with an alternating magnetization profile was fabricated as shown in Figure 3e. Upon the application of a uniform magnetic field of 100 mT, the straight sheet transforms into an "s" shape instantly,

which was in good agreement with the FEA simulation results. The actuating stability was assessed by cyclically applying a uniform magnetic field to PDMS-NdFeB sheets with uniform and nonuniform magnetization profiles (Figure 3f). A stable actuation output was confirmed through 2000 cycles for both cases. The actuation rate for the uniform magnetization profile was measured to be 35.8 mm $s^{-1}$ in terms of the vertical uprise under a quasi-transient horizontal magnetic field of 20 mT (detailed information in Figure S14, Supporting Information). The highly resilient mechanical properties of the actuating layer, together with the robust hue-tuning capability, cooperatively empowered repeatable and durable shape-color programming of the SoMMeC structures.

### 2.4. SoMMeC Robots with Programmable Dynamic Advertising Iridescence and Adaptive Camouflage

Some animals can actively change their skin coloration for attraction or camouflage. To mimic the skill, we designed the SoMMeC-based caterpillar robot and rolling robot with programmable locomotion and coloration by tailoring the dimensions and magnetization profiles (**Figure** 4a(i) and Figure S15, Supporting Information). Based on the MMC coupling map derived from the predictive model (e.g., the MMC coupling map for radial magnetization case in Figure 4a(ii)), the shape-color prediction could be obtained from simulation results (Figure 4a(iii) and Figure S16, Supporting Information): The caterpillar robot with sinusoidal magnetization transformed from flat and yellow into a wavy and iridescent appearance across the body length under a uniform magnetic field; The rolling robot with radial magnetization transformed from flat and yellow into a concave and red, or convex and blue, hemispherical shape under an upward or downward uniform magnetic field.

Upon a programmed rotating magnetic field, the caterpillar robot delivered undulating crawling locomotion, accompanied by a continuously changing iridescent skin (Movie S2, Supporting Information). The rotating magnetic field could produce a longitudinal traveling wave across the robot's body length. Assisted by the friction between the two ends of the robot with the ground, the traveling wave would propel the robot to move in the same direction as the body wave transmission. The undulatory crawling locomotion strategy was schemed in the Figure S17 (Supporting Information). Figure 4b(i) records the body hue profile of the caterpillar robot during locomotion, featuring a spatiotemporally dynamic hue tuning along the body length. Such advertising coloration for soft robots can serve not only for attractive or aposematic purposes but also for color-encoded signaling upon choreographed magnetic input. For the rolling robot, adjusting the direction and magnitude of the applied magnetic field gave access to a full-visible-spectrum robot color tunability (Figure S18 and Movie S3, Supporting Information). Such efficient body-color switching inspired a camouflaging strategy: the robot locomoted by rolling and adapted its body color to the varying backgrounds (Movie S4, Supporting Information). Figure 4b(ii) displays that the rolling robot kept a minimal robot-background hue deviation during the locomotion on different backgrounds. We deployed the rolling robot in a simulated forest environment with leaves and petals (Figure 4c): Under an adjusted magnetic field based on the predictive model, the robot changed its color to blend in with the red petals, confirmed by a close resemblance of the three-channel RGB histograms between the background and self-camouflaged states. Noteworthy is that the SoMMeC robot accomplished a full-visible-spectrum color shift with a minimal lateral dimension variation (Figure S19, Supporting Information), avoiding the large uniaxial tensile strain required by conventional mechano-chromic structures[17,45,50,51] (typically above 60%). The minimal lateral size adjustment is favorable for inconspicuous concealment. Furthermore, the shape-color tuning of the SoMMeC robot could be exploited in more application scenarios through specific modification. For instance, a strip-shaped SoMMeC rolling robot with conductive coating could serve as a remote steering "circuit patch" with a visual positioning marker to repair damaged electric circuits where manual operation is inaccessible (Figure S20, Supporting Information).

### 2.5. SoMMeC Gripper with Visual Feedback Sensing

The perception of gripping status is indispensable for accurate grasping control. Visual sensing related to color change can supplement conventional digital sensing, or relieve the compact soft gripper from the need for sophisticated electronic or mechanical sensors. We assembled a SoMMeC soft gripper with three photonic crystal films on top of each arm to act as structural-color pixels (PC pixels) for visual self-sensing (**Figure** 5a and detailed magnetization profile in Figure S21, Supporting Information): The gripper and cargo were placed on an operation table, and a white LED light was applied from top and a camera was set by the side to record the structural color variation. A magnet of adjustable magnetic intensity was fixed onto an industrial robotic arm under the operation table to translate or rotate in a predefined procedure for different shape-morphing or locomotion types (Figure S22, Supporting Information). As the magnetic field intensity increased from 0 to 180 mT, the gripping angle $\beta$ increased and the PC pixels changed the colors, as shown in the simulated and experiment results from Figure 5b (Movie S5, Supporting Information). Here the structural color variation was due to the bending-induced change of both the PC lattice spacing and the viewing angle. To quantitatively measure the gripping angle, we adopted the hue channel from HSV (hue, saturation, value) color space using a simple imaging tool (e.g., a smartphone camera), rather than sophisticated hyperspectral imaging equipment, to make it a simple and feasible method. Figure 5c displays the gripping angle dependence of the PC pixels hues. The PC pixel hue change proved stable and durable through 1000 cycles of magnetically controlled gripping (Figure 5d). The set of PC pixel hues could serve as a colorimetric indicator of the gripping angle. For example, when the SoMMeC gripper grasped cylinder-shaped cargos of varying sizes (Figure 5e, Movie S6, Supporting Information), the set of the PC pixels hues at the fastening state varied from each other, suggesting the gripping angles of 38, 68, and 72 degrees according to the calibration curves. The SoMMeC gripper could grab a maximal weight of 4 g under a magnetic field of 180 mT, which was 8 times its own weight. Interestingly, the SoMMeC gripper could also identify different cargo shapes (e.g., cylinder, tetrahedron, cube, and crescent moon shapes) via the hue combinations of the four sets of PC pixels from the gripper arms,

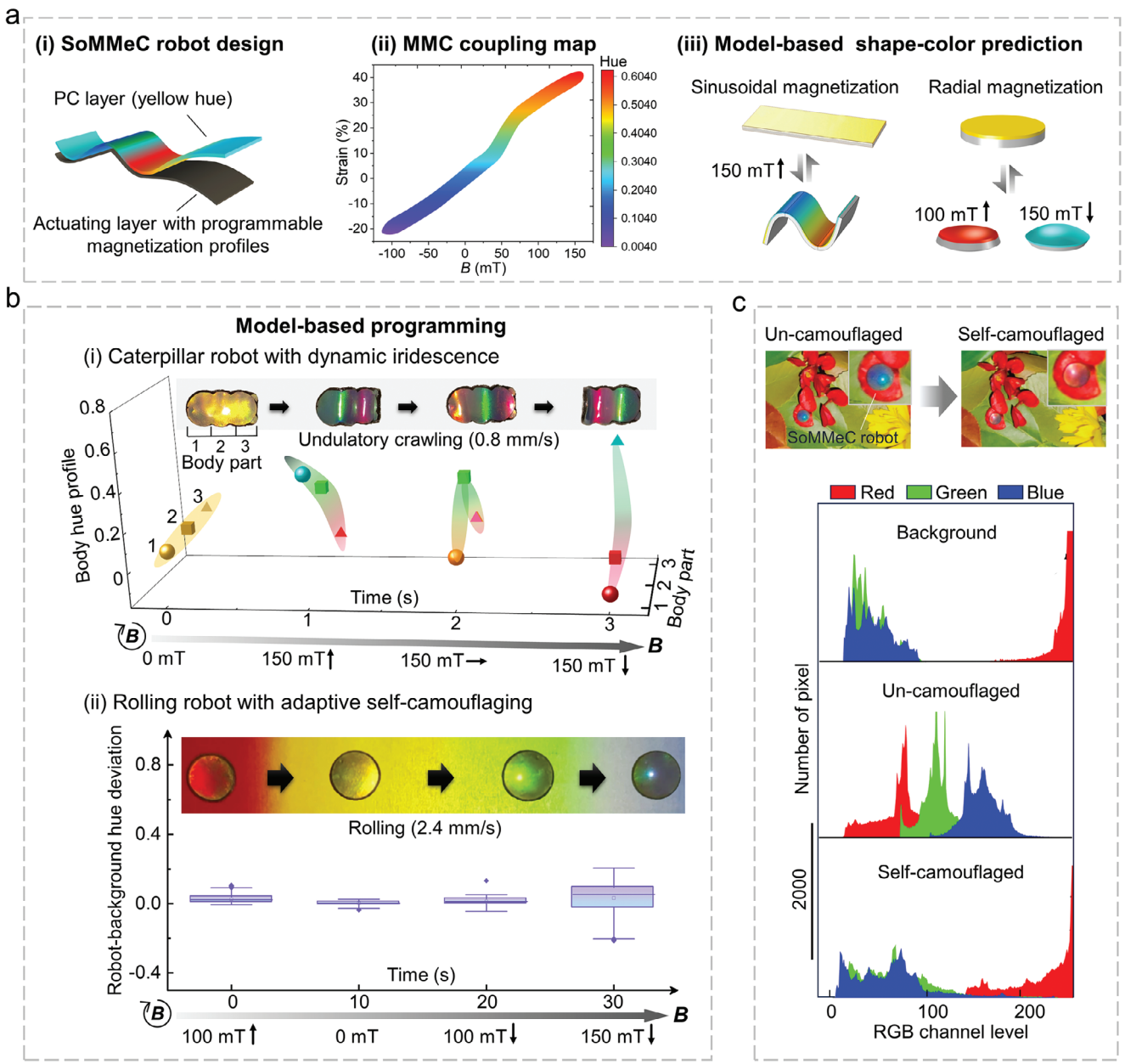


**Figure 4.** SoMMeC robots with programmable locomotion and coloration. a) i) The structural illustration of SoMMeC robots with programmable magnetization profiles; ii) The MMC coupling map derived from the predictive model of the radial magnetization case; iii) The model-based shape-color prediction of SoMMeC robots with sinusoidal (caterpillar robot) and radial (rolling robot) magnetization. b) i) The hue profile variation of the caterpillar robot body (divided into three parts) during undulatory crawling. The inset shows the crawling robot with iridescence. ii) The hue deviation between the rolling robot and the background during the rolling locomotion. The inset shows the rolling robot with adaptive self-camouflage. c) Photographs of SoMMeC robot at un-camouflaged and self-camouflaged states (top); Corresponding RGB histogram of the background, non-camouflaged, and self-camouflaged states (bottom).

wherein the cargo geometries directly affect the bending states of each gripper arm and the corresponding hues (detailed information in Figure S23, Supporting Information). Considering the low cost of analyzing color data and the high sampling rate by a commonly available camera, the hue channel-enabled motion sensing can serve as a cost-effective and real-time monitoring platform for robotic locomotion and manipulation. Besides, the SoMMeC gripper is also ready for functional upgradability by integration with other conventional materials. For instance, multi-walled carbon nanotube (MWCNT) percolation film could be assembled to provide piezoresistive sensing of the gripping angle to supplement the colorimetric indicator when the lighting condition is unsatisfactory (detailed information in Figure S24, Supporting Information).

By integrating the SoMMeC gripper into an industrial robotic arm, the grasping and self-sensing can be exploited for

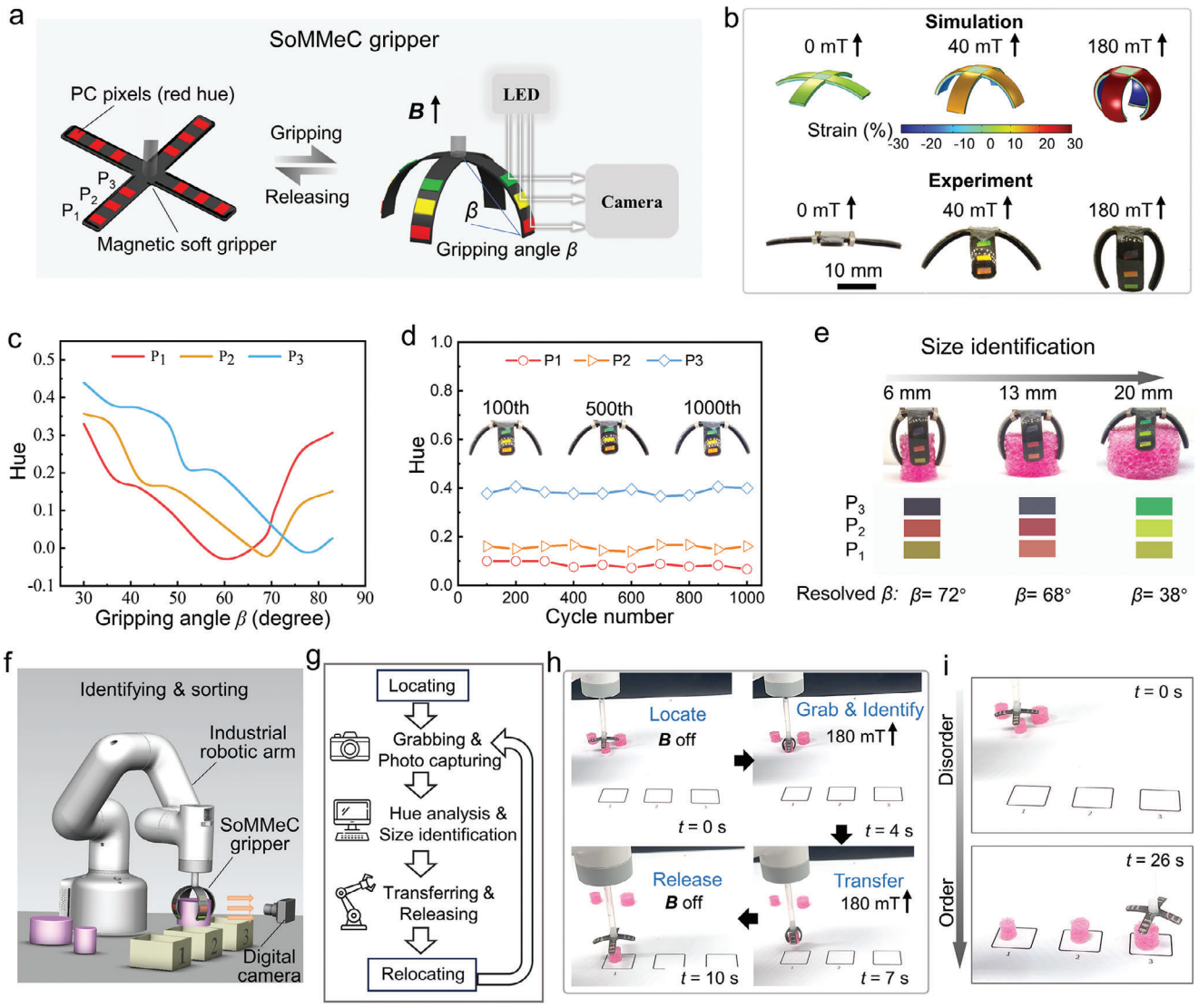


**Figure 5.** SoMMeC gripper with visual feedback self-sensing. a) The magnetically controlled gripping and hue-recording setup of the SoMMeC gripper. b) Simulation and experimental results of the gripping angle increase under a uniform magnetic field from 0 to 180 mT. c) The dependence of the PC pixels hues on the gripping angle. d) The PC pixels hues variation during 1000 magnetic actuation cycles at 40 mT. e) The PC pixels hues when grasping cargos of varying size and the calculated gripping angle. The weight of the cylinder-shaped foam cargo was 20, 100, and 220 mg for the diameters of 6, 13, and 20 mm respectively. f) Schematic of the robot-assisted SoMMeC gripper for cargo identifying and sorting. g) The operational flow chart of the SoMMeC gripper. h) The process of grasping, analyzing, and transferring using the robot arm-assisted SoMMeC gripper. i) The SoMMeC gripper enabled the transport and classification of chaotically placed cargo.

complicated tasks such as cargo identification and sorting (Figure 5f). The operational procedure is shown in Figure 5g (detailed process in Note S3, Supporting Information). The robotic arm could locate the SoMMeC gripper to the cargo to allow the grasping and size identification controlled by a magnetic field of 180 mT. The measured size was utilized for further transferring and sorting (Figure 5h). Thus, the SoMMeC gripper with automated visual-sensing and actuation feedback could wirelessly classify and sort chaotically placed cargo into an ordered state according to the size (Figure 5i and Movie S7, Supporting Information).

### 2.6. SoMMeC Platform for Information Hiding and Encryption

The capability of predictable multi-color transformation of the SoMMeC structure suggested a promising alternative for information hiding and encryption. Image information could be magnetically written into a carbon black-PDMS (CB-PDMS) sheet using NdFeB-PDMS as the magnetic ink, as illustrated in **Figure 6**a(i) (detailed magnetization profile in Figure S25, Supporting Information). An S-shaped pattern, as shown in Figure 6a(ii), transformed between a displayed state under an applied magnetic field (***B*** on) and a hidden state (***B*** off) and could

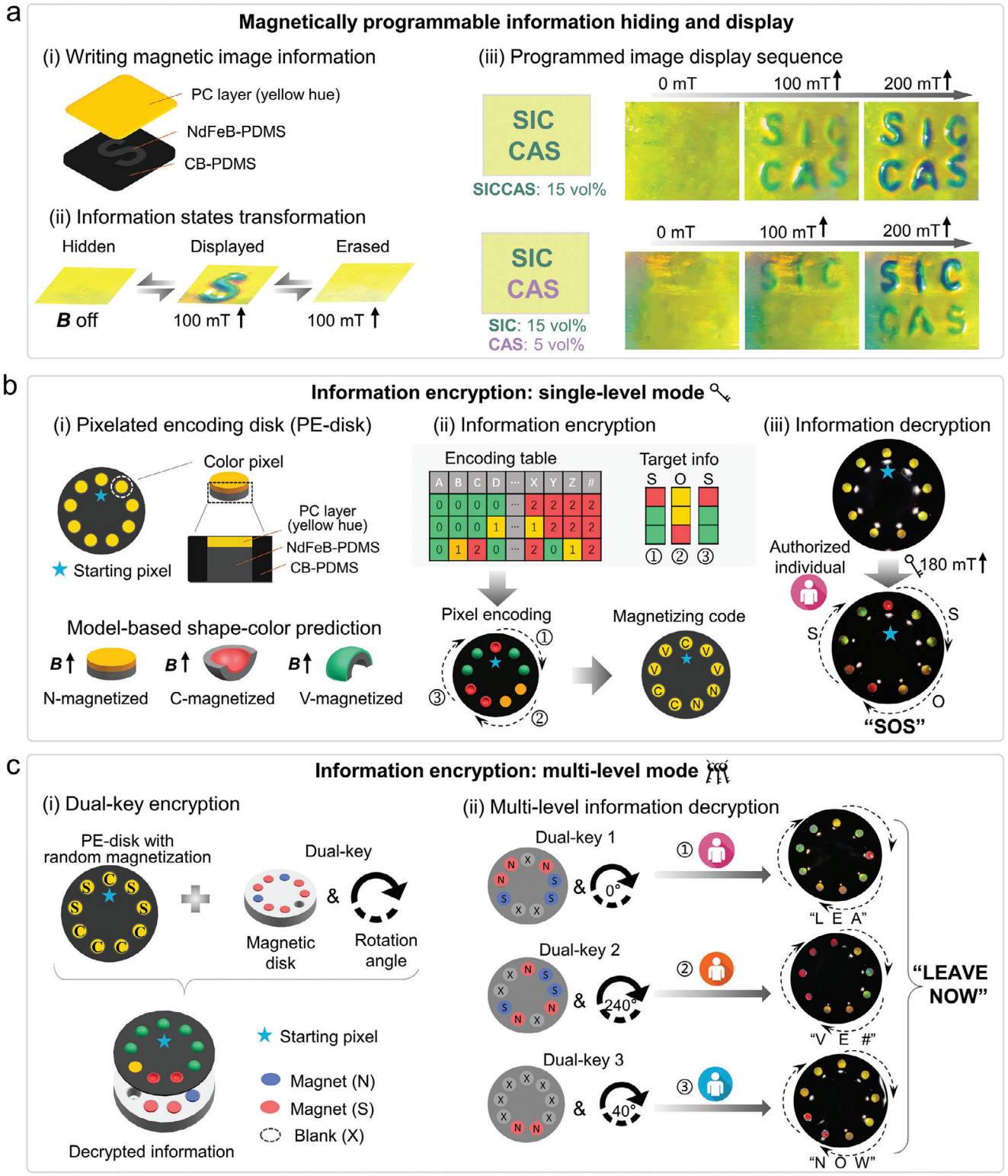


**Figure 6.** SoMMeC platform for information hiding and advanced encryption. a) Information hiding platform including i) the explosive-view configuration, ii) photographs of information state transformation, and iii) magnetically programmable display sequence of image information. b) Single-level mode information encryption including i) the structure of the PE-disk and model-based color prediction, ii) the encryption algorithm of target information "SOS", and iii) the information decryption of "SOS" using a uniform magnetic field of 180 mT. c) Multi-level mode information encryption including i) the dual-key design to decrypt information from a PE-disk with random magnetization, and ii) multiple authorized individuals sequentially and collectively decrypted the correct information "LEAVE NOW".

be erased using a decreasing oscillating magnetic field. The display sequence could be programmed by tuning the magnetic ink and the magnetic field: Under an increasing magnetic field, the letters "SICCAS" with a single magnetic ink (NdFeB volume content of 15 vol%) started to appear at 100 mT and bolder at 200 mT; For magnetic inks of varying compositions (15 vol% for "SIC", 5 vol% for "CAS"), the "SIC" first emerged at 100 mT, followed by the "CAS" at 200 mT. The image hiding and programmable display sequence can be potentially utilized in anti-counterfeiting labels.

For information encryption, we devised a SoMMeC-based pixelated encoding disk (PE-disk) with nine PC pixels. Under an upward magnetic field, the PC pixels exhibited hues of yellow, red, and green with different magnetization profiles of non-magnetized (N-magnetized), concavely magnetized (C-magnetized), and convexly magnetized (V-magnetized) respectively, as shown in Figure 6b(i). We predefined an encoding table (Figure S26, Supporting Information) to cover the alphabet, whereby a set of three colors indicated a specific letter. 27 available sets could be assigned to 26 letters and a number sign "#" as a space between letters. The PE-disk accommodated 3 sets of pixels from the starting pixel. The targeted information (for instance, "SOS") was encoded into the PE-disk by adjusting the magnetization profiles(N-/C-/V-magnetized) of each pixel, comprising a magnetizing code for the PE-disk (Figure 6b(ii)). An authorized individual with the encryption algorithm (the encoding table) could decrypt the information by applying an upward magnetic field of 180 mT to the PE-disk, representing a single-level mode information encryption, as shown in Figure 6b(iii).

To further enhance the security level, a multi-level encryption scheme was developed. Instead of a uniform magnetic field, a dual-key, comprised of a magnetic disk and a rotation angle relative to the PE-disk, was employed to decode the information from a PE-disk with random magnetization profiles (Figure 6c(i)). The magnetic disk consisted of nine magnets with a northpole upward (N) downward (S) or blank (X). Only with a correct assembly of magnets and a correct rotation angle $\alpha$, the targeted information could be correctly decrypted by applying the magnetic disk to the PE-disk. A confidential message could be broken up and encoded into multiple dual keys for multiple authorized individuals. For example, three authorized individuals with three dual keys (magnetic disk and rotation angle), could independently decode part of the target information, and collectively compose a decrypted information of "LEAVE NOW" (Figure 6c(ii)). Upon receiving incorrect keys (magnetic disk of incorrect magnets assembly or incorrect rotation angle), the multi-level mode encryption system would generate fake information to deceive the unauthorized attackers (Figure S27, Supporting Information).

## 3. Conclusion

Integration of shape-morphing and color-changing in soft structures promises sophisticated robotic and sensing applications, but previous trials face the issues of slow response, limited coloration choice, and model-predictable programming. In this work, we successfully mimic the chameleon's color-tuning mechanism to propose a two-layered SoMMeC structure composed of nonsolvent photonic film and magnetic actuating film. The synergistic MMC coupling enabled fast, dynamic, tether-free, and programmable shape-color tunability. The SoMMeC structure was mechanically robust to endure stretch, bend, and twist deformations, and also functionally robust to sustain thermo-mechanical impacts with consistent color-tuning and shape-morphing properties. A predictive model was established based on mechanical FEA and strain-dependent color evolving map, to provide the shape-color changes with various geometrical configurations and magnetization profiles. To demonstrate the potential of robotic-visual applications, we showcased SoMMeCS-based locomotive robots with dynamic advertising coloration and adaptive camouflaging, a soft gripper with visual feedback self-sensing, and an encoding platform for information hiding and encryption.

These prototypes show how this unique SoMMeC structure could unleash the untapped potential for hybrid robotic and visual systems that require compact design, mechanical compliance, high robustness, and multimodal functionality. In the future, we can envision the incorporation of magnetic ink 3D printing to achieve more complex and customizable geometrical transformation and dynamic coloration.[42,52] Beyond pure bending-induced shape change, more complex shape morphing could be achieved by using a kirigami strategy. Predefined cutting patterns in planar SoMMeC structures could transform into 3D architecture involving bending and twisting deformation modes upon magnetic simuli (3D helical shape as an example in Figure S28, Supporting Information). Also, instead of an inactive PDMS matrix, a phase transition polymer could serve as a shape-locking element for localized structure adjustment independent of the global geometry and homogeneous magnetization profile, to enrich the programming space of complex SoMMeC structures (thermal phase transitional polymer as an example in Figure S29, Supporting Information). In this work, we selected the reflected color in a normal direction and neglected the viewing-angle effect, for structural color analysis, as we here focused on the investigation of synergistic MMC coupling for shape-color programming. If demanded by specific scenarios, the photonic crystal film could readily be engineered to gain a viewing angle-independent structural color to eliminate the observing angle influence.[53,54] Besides the shape-morphing induced strain, other stimuli that could bring about considerable dimensional variation of the photonic film would also affect the color-changing performance, such as the organic solvent that could swell the PC film. An extra coating of inert polymer on the PC film could be a possible solution. For locomotion tasks in open spaces with a large motion range (e.g., field exploration robots), the current on-site magnetic source would be unqualified. Integrating an onboard magnetic input module into the robotic system is a promising avenue, however, it raises higher demand for robot design and assembly to avoid interference from the onboard magnetic module. Mechanical vibrations in the surroundings can affect the accurate transfer of strain distribution on the SoMMeC structure, resulting in a disturbed shape-color response. Adoption of a cushion pad at the operation site or an increase in the robot size could facilitate the SoMMeC robot to withstand violent mechanical disturbances. In terms of the control system, the SoMMeC crawling and rolling robots belong to the feedforward type as the magnetic input was predetermined based on the pre-evaluated environmental factors of interest; The SoMMeC gripper features a feedback control as an on-site

camera system that automatedly recorded the hues of PC pixels in real-time to adjust the magnetic input programming for smart identification and transportation. Another alternative strategy to accomplish a closed-loop feedback control system is to integrate on-board sensing and analyzing modules into the robotic system, which is more demanding due to the increased complexity of the robot design to avoid interference from the alien components.

## 4. Experimental Section

*Materials*: Tetraethyl orthosilicate (TEOS, Shanghai Titan Technology), carbon black (CB, average particle size: 30–45 nm, Xianfeng Nanomaterials Technology), aqueous ammonia (Sinopharm Chemical Reagent), polyethylene glycol phenyl ether acrylate (PEGPEA, MW324, Sigma–Aldrich), di(ethylene glycol) ethyl ether acrylate (DEGEEA, MW188, Sigma–Aldrich), polyethylene glycol diacrylate (PEGDA, MW700, Shanghai Macklin Biochemical Technology), 2-hydroxy-2-methylphenylacetone (Irgacure1173, Adamas), poly dimethylsiloxane (PDMS, Sylgard184, Dow Corning), NdFeB particles (average diameter: 5 µm, Megacun International Trading), and multi-wall carbon nanotubes (MWCNT, 40–60 nm, Chengdu Jiacai Technology). All chemicals were used directly without further purification.

*Preparation of the Photonic Crystal Thin Film*: $SiO_2$ nanospheres with different particle sizes were prepared by the modified Stober method. 0.02 mL $SiO_2$ (5 vol% in ethanol) was re-dispersed in ethanol solution containing 0.03 mL DEGEEA and 0.03 mL PEGPEA. Then 2-hydroxy-2-methylphenylacetone with a monomer content of 0.5vol% was added as a photo initiator and PEGDA with a monomer content of 1vol% was added as a crosslinking agent. The solution was dried in an oven at 80 °C for 10 h to completely remove ethanol to obtain 0.08 mL precursor solution. Next, polyimide tape (Kapton) was attached between two glass slides to form a 50 um gap, and drops of the precursor solution were added to permeate into the gap. After photocuring under UV light (356 nm) irradiation for 50 s, the photonic crystal film was obtained.

*Preparation of the Magnetic Actuating Layer*: The NdFeB particles and PDMS precursor (base and curing agents at a weight ratio of 30:1) were mixed at different NdFeB volume ratios (5 vol%, 10 vol%, 15 vol%). After degassing in a vacuum chamber, the mix was poured into a mold with a thickness of 1mm. Then, it was cured in an oven at 110 °C for 20 min, and cut into different patterns as demanded. The PDMS-NdFeB elastomers could be bent into desired shapes by a template-assisted method and magnetized using a pulsed magnetic field of ≈2.5 T (magnetizer, MAG-2070, Shenzhen Heshenghui Electronics).

*Fabrication of Locomotive Robots Based on SMMCS*: A small amount of PDMS precursor solution (base to curing agents at a weight ratio of 30:1) was spin-coated on the surface of the magnetic actuating layer to act as a thin glue layer. Then a photonic film was attached to the surface of the magnetic actuating layer. After degassing in a vacuum chamber, the two-layered structure was cured in an oven at 110 °C for 20 min with a compression force. After curing, the two-layered structure could be cut into desired patterns and magnetized to get locomotive crawling and rolling soft robots with dynamic coloration and self-camouflage, respectively. To trigger the locomotion, a magnet or electromagnetic coil was fixed to an industrial robotic arm under or above the operation site. The magnet could be controlled to translate or rotate in a predefined procedure to exert a programmable magnetic field. The magnetic field intensity at different distances from the magnet was calibrated by a digital gauss meter (ZMST-1) before experiments.

*Fabrication of the Soft Gripper with Dual-Signal Feedback Sensing*: After the magnetization of the magnetic layer was completed, the magnetic layer was treated with oxygen plasma (power of 100 W) for 20 s. Polyimide tape was used as a mask to form a U-shaped pattern on the surface of the magnetic layer. The surface of the magnetic actuating layer was then sprayed with MWCNT on a heating stage at 100 °C to form a U-shaped MWCNT-sensor. Conductive tape was connected to the MWCNT-sensor using adhesive silver paste. Then three photonic film pixels with an initial hue of red were attached and fixed to the surface of the gripper arms using PDMS precursor solution as curable glue.

*Fabrication of the Encoding Platform for Information Hiding and Encryption*: Carbon black was dispersed in isopropyl alcohol (iPOH) and homogenized by ultrasonic treatment. A uniform CB-iPOH suspension was mixed with PDMS base prepolymer. The iPOH was evaporated in an oven at 80 °C. Then PDMS curing agent (weight ratio of 30:1) was added to get a PDMS-CB precursor solution with 1wt.% CB. The PDMS-CB precursor was degassed and poured into a disk-shaped mold, and SMMCS-based color pixels were fixed ringwise into the PDMS-CB precursor solution, followed by curing in an oven at 110 °C for 20 min. For information writing, the printing method was adopted to prepare a magnetic actuating layer (the ink of NdFeB and PDMS precursor solution) with desired patterns for magnetically controlled information hiding. A syringe nozzle was used to extrude specific patterns with the help of a digitalized translational stage. The printing resolution limit was 1 mm, limited by the manual assembly of PC film assembly to the magnetic actuating layer.

*Characterization*: Morphology characterization was conducted using a field emission scanning electron microscope (FESEM, SU8010, Hitachi, Japan). The particle size distribution of $SiO_2$ was measured by dynamic light scattering (DLS, 90PlusPALS, Brookhaven, USA). Zeta potential was measured by electrophoretic light scattering method with ethanol as a dispersive medium. The reflectance spectrum was measured by an UV–vis spectrophotometer (LAMBDA1050, PerkinElmer Instruments, USA). The infrared spectrum was collected using an infrared spectrometer (Spotlight 400, PE, USA). The temperature-variable FTIR spectrum was tested by in situ infrared (NicoletiS50, Thermo Fisher Scientific) with a temperature range of 25–85 °C at a temperature interval of 10 °C and a holding time of 5 min. The mechanical tests were conducted on a universal material testing machine (CMT6103, Metus Industrial Systems China). For determining the basic mechanical properties of the materials, samples (the magnetic actuating material, the photonic film, and the SoMMeC structure) were tested at a strain rate of 0.03 mm $s^{-1}$. The rectangular samples had a length of 15 mm, a width of 5 mm, and a gauge length of 10 mm. Young's modulus was calculated from the tensile stress–strain slope at a low strain range (within 5% strain). For the strain measurement of the complex 3D SoMMeC structure under a magnetic field, numerical simulation was utilized to calculate the localized strain distribution of the SoMMeC structure. The hysteresis loop of the magnetic elastomer was measured using a vibrating sample magnetometer (VSM, Lakeshore7410, lakeshore, USA). RGB histograms of 3 channels were plotted using MATLAB software to evaluate the color similarity of different backgrounds.

## Supporting Information

Supporting Information is available from the Wiley Online Library or from the author.

## Acknowledgements

X.L. and Y.C. contributed equally to this work. This work was supported by the Shanghai International Science and Technology Cooperation Project (23520711000) from the Science and Technology Commission of Shanghai Municipality, National Natural Science Foundation of China (52203365, 62122080, 62471459, 62261136551) and A*STAR, RIE2025 Manufacturing, Trade and Connectivity (MTC), M22K2c0081.

## Conflict of Interest

The authors declare no conflict of interest.

## Data Availability Statement

The data that support the findings of this study are available from the corresponding author upon reasonable request.

## Keywords

color-tuning, dynamic control, shape-shifting, soft robots, synergistic coupling

Received: May 10, 2024
Revised: October 28, 2024
Published online: November 9, 2024

[1] Y. Forterre, J. M. Skotheim, J. Dumais, L. Mahadevan, *Nature* **2005**, *433*, 421.
[2] M. Moriyama, in *Pigments, Pigment Cells and Pigment Patterns*, (Eds: H. Hashimoto, M. Goda, R. Futahashi, R. Kelsh, T. Akiyama), Springer, Singapore **2021**.
[3] D. Rus, M. T. Tolley, *Nature* **2015**, *521*, 467.
[4] S. I. Rich, R. J. Wood, C. Majidi, *Nat. Electron.* **2018**, *1*, 102.
[5] X. Q. Wang, C. F. Tan, K. H. Chan, X. Lu, L. Zhu, S. W. Kim, G. W. Ho, *Nat. Commun.* **2018**, *9*, 3438.
[6] Y. Yang, Y. Wu, C. Li, X. Yang, W. Chen, *Adv. Intel. Sys.* **2020**, *2*, 1900077.
[7] Y. Cheng, K. H. Chan, X. Q. Wang, T. Ding, T. Li, X. Lu, G. W. Ho, *ACS Nano* **2019**, *13*, 13176.
[8] J. Shintake, V. Cacucciolo, D. Floreano, H. Shea, *Adv. Mater.* **2018**, *30*, 1707035.
[9] S. Song, D. M. Drotlef, D. Son, A. Koivikko, M. Sitti, *Adv. Sci.* **2021**, *8*, 2100641.
[10] Y. Cheng, R. Wang, K. H. Chan, X. Lu, J. Sun, G. W. Ho, *ACS Nano* **2018**, *12*, 3898.
[11] W. Liu, Y. Duo, J. Liu, F. Yuan, L. Li, L. Li, G. Wang, B. Chen, S. Wang, H. Yang, Y. Liu, Y. Mo, Y. Wang, B. Fang, F. Sun, X. Ding, C. Zhang, L. Wen, *Nat. Commun.* **2022**, *13*, 5030.
[12] Y. Qiu, S. Sun, X. Wang, K. Shi, Z. Wang, X. Ma, W. Zhang, G. Bao, Y. Tian, Z. Zhang, H. Ding, H. Chai, A. Liu, H. Wu, *npj Flexible Electron.* **2022**, *6*, 45.
[13] M. Li, Y. Tang, R. H. Soon, B. Dong, W. Hu, M. Sitti, *Sci. Adv.* **2022**, *8*, eabm5616.
[14] I. C. Yasa, H. Ceylan, U. Bozuyuk, A. M. Wild, M. Sitti, *Sci. Rob.* **2020**, *5*, eaaz3867.
[15] A. C. Siegel, S. T. Phillips, B. J. Wiley, G. M. Whitesides, *Lab Chip* **2009**, *9*, 2775.
[16] C. Yu, Y. Li, X. Zhang, X. Huang, V. Malyarchuk, S. Wang, Y. Shi, L. Gao, Y. Su, Y. Zhang, H. Xu, R. T. Hanlon, Y. Huang, J. A. Rogers, *Proc. Natl. Acad. Sci. USA* **2014**, *111*, 12998.
[17] B. H. Miller, H. Liu, M. Kolle, *Nat. Mater.* **2022**, *21*, 1014.
[18] Y. Jin, Y. Lin, A. Kiani, I. D. Joshipura, M. Ge, M. D. Dickey, *Nat. Commun.* **2019**, *10*, 4187.
[19] Y. Ma, Y. Yu, P. She, J. Lu, S. Liu, W. Huang, Q. Zhao, *Sci. Adv.* **2020**, *6*, eaaz2386.
[20] Z. Man, Z. Lv, Z. Xu, Q. Liao, J. Liu, Y. Liu, L. Fu, M. Liu, S. Bai, H. Fu, *Adv. Funct. Mater.* **2020**, *30*, 2000105.
[21] S. A. Morin, R. F. Shepherd, S. W. Kwok, A. A. Stokes, A. Nemiroski, G. M. Whitesides, *Science* **2012**, *337*, 828.
[22] T. Ranzani, S. Russo, N. W. Bartlett, M. Wehner, R. J. Wood, *Adv. Mater.* **2018**, *30*, 1802739.
[23] S. Wu, H. Shi, W. Lu, S. Wei, H. Shang, H. Liu, M. Si, X. Le, G. Yin, P. Theato, T. Chen, *Angew. Chem., Int. Ed.* **2021**, *60*, 21890.
[24] S. Wei, W. Lu, X. Le, C. Ma, H. Lin, B. Wu, J. Zhang, P. Theato, T. Chen, *Angew Chem Int Ed Engl* **2019**, *58*, 16243.
[25] C. Ma, W. Lu, X. Yang, J. He, X. Le, L. Wang, J. Zhang, M. J. Serpe, Y. Huang, T. Chen, *Adv. Funct. Mater.* **2018**, *28*, 1704568.
[26] C. Larson, B. Peele, S. Li, S. Robinson, M. Totaro, L. Beccai, B. Mazzolai, R. Shepherd, *Science* **2016**, *351*, 1071.
[27] P. Zhang, I. M. Lei, G. Chen, J. Lin, X. Chen, J. Zhang, C. Cai, X. Liang, J. Liu, *Nat. Commun.* **2022**, *13*, 4775.
[28] C. Li, Q. He, Y. Wang, Z. Wang, Z. Wang, R. Annapooranan, M. I. Latz, S. Cai, *Nat. Commun.* **2022**, *13*, 3914.
[29] J. Ma, Y. Yang, C. Valenzuela, X. Zhang, L. Wang, W. Feng, *Angew. Chem., Int. Ed.* **2022**, *61*, 202116219.
[30] P. Zhang, M. G. Debije, L. T. de Haan, A. P. H. J. Schenning, *Acs Appl Mater Inter* **2022**, *14*, 20093.
[31] H. Kim, J. Choi, K. K. Kim, P. Won, S. Hong, S. H. Ko, *Nat. Commun.* **2021**, *12*, 4658.
[32] Y. Wang, H. Cui, Q. Zhao, X. Du, *Matter* **2019**, *1*, 626.
[33] P. Xue, Y. Chen, Y. Xu, C. Valenzuela, X. Zhang, H. K. Bisoyi, X. Yang, L. Wang, X. Xu, Q. Li, *Nano-Micro Lett.* **2022**, *15*, 1.
[34] Z. Hao, S. Song, B. Li, Q. X. Jia, T. Zheng, Z. Zhang, *Sens. Actuators, B* **2022**, *358*, 131448.
[35] X. Du, H. Cui, T. Xu, C. Huang, Y. Wang, Q. Zhao, Y. Xu, X. Wu, *Adv. Funct. Mater.* **2020**, *30*, 1909202.
[36] L. Peng, Y. Zhang, J. Wang, Q. Wang, G. Zheng, Y. Li, Z. Chen, Y. Chen, L. Jiang, C. P. Wong, *Nano Energy* **2022**, *99*, 107367.
[37] T. Wu, X. Wang, X. Cao, N. Wang, *Nano Energy* **2024**, *128*, 109883.
[38] T. Zhang, Y. Ding, C. Hu, M. Zhang, W. Zhu, C. R. Bowen, Y. Han, Y. Yang, *Adv. Mater.* **2023**, *35*, 2203786.
[39] M. PourhosseiniAsl, A. Berbille, S. Wang, Z. Yu, Z. Li, K. Ren, S. Dong, *Adv. Mater. Interfaces* **2023**, *10*, 2202332.
[40] M. C. Wong, L. Chen, M. K. Tsang, Y. Zhang, J. Hao, *Adv. Mater.* **2015**, *27*, 4488.
[41] J. Teyssier, S. V. Saenko, D. van der Marel, M. C. Milinkovitch, *Nat. Commun.* **2015**, *6*, 6368.
[42] Y. Kim, H. Yuk, R. Zhao, S. A. Chester, X. Zhao, *Nature* **2018**, *558*, 274.
[43] Y. Cheng, K. H. Chan, X. Q. Wang, T. Ding, T. Li, C. Zhang, W. Lu, Y. Zhou, G. W. Ho, *Adv. Funct. Mater.* **2021**, *31*, 2101825.
[44] Y. Zhao, Z. Xie, H. Gu, C. Zhu, Z. Gu, *Chem. Soc. Rev.* **2012**, *41*, 3297.
[45] G. H. Lee, T. M. Choi, B. Kim, S. H. Han, J. M. Lee, S. H. Kim, *ACS Nano* **2017**, *11*, 11350.
[46] Y. Hu, B. Wei, D. Yang, D. Ma, S. Huang, *Acs Appl Mater Inter* **2022**, *14*, 11672.
[47] S. H. Kim, H. S. Park, J. H. Choi, J. W. Shim, S. M. Yang, **2010**, *22*, 946.
[48] Y. Kim, X. Zhao, *Chem. Rev.* **2022**, *122*, 5317.
[49] G. Mao, D. Schiller, D. Danninger, B. Hailegnaw, F. Hartmann, T. Stockinger, M. Drack, N. Arnold, M. Kaltenbrunner, *Nat. Commun.* **2022**, *13*, 4456.
[50] E. Miwa, K. Watanabe, F. Asai, T. Seki, K. Urayama, J. Odent, J. M. Raquez, Y. Takeoka, *ACS Appl. Polym. Mater* **2020**, *2*, 4078.
[51] T. H. Park, S. Yu, S. H. Cho, H. S. Kang, Y. Kim, M. J. Kim, H. Eoh, C. Park, B. Jeong, S. W. Lee, D. Y. Ryu, J. Huh, C. Park, *NPG Asia Mater.* **2018**, *10*, 328.
[52] D. Wang, J. Wang, Z. Shen, C. Jiang, J. Zou, L. Dong, N. X. Fang, G. Gu, *Annu. Rev. Control Robot. Auton. Syst.* **2023**, *6*, 31.
[53] H. Tan, Q. Lyu, Z. Xie, M. Li, K. Wang, K. Wang, B. Xiong, L. Zhang, J. Zhu, *Adv. Mater.* **2019**, *31*, 1805496.
[54] G. Bae, M. Seo, S. Lee, D. Bae, M. Lee, *Adv. Mater. Technol.* **2021**, *6*, 2100118.